Computational Materials Science 137 (2017) 113–118

Contents lists available at ScienceDirect

Computational Materials Science

journal homepage: www.elsevier.com/locate/commatsci

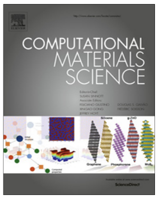

An improved method to predict the Wulff shape: An example for Li_2CoSiO_4

Ming Xu, Jinlong Yang, Jiaxin Zheng*, Feng Pan*

School of Advanced Materials, Peking University Shenzhen Graduate School, Shenzhen 518055, China

A R T I C L E I N F O

Article history:
Received 17 March 2017
Received in revised form 12 May 2017
Accepted 13 May 2017

Keywords:
Wulff construction
Density functional theory
Multivariate linear regression
Li_2CoSiO_4

A B S T R A C T

The Wulff construction based on surface energy calculations is an effective tool to understand and predict the shape of nanoparticles. Previous surface energy calculation faces the challenge to precisely deal with the dipole electric field in a slab. Here we propose a method that by fitting the calculated surface energies with no dipole electric field through multivariate linear regression, the separate contributions to the surface energy from the cations coordination loss terms on the surface can be obtained. The fitted results can further be used to estimate the surface energies of slabs with dipole electric field directly and accurately. Using this method, the Wulff shapes of three phases of Li_2CoSiO_4, a kind of materials with great potential for oxygen evolution reaction (OER) electrocatalysts, are precisely constructed.

1. Introduction

The surface properties of small particles play great roles on catalysis, gas sensing [1], and chemisorption [2]. Thus a detailed understanding of the morphologies of small particles is important. Wulff construction, originated from the experimental observation of natural crystals by Wulff and the quantitative explanations boosted by von Laue, Dinghas and Herring [3], is able to identify the thermodynamic stable clusters and predict the shape of nanoparticles, including single crystal, alloy [1,3–5], etc. Now it is widely used in nanotechnology to understand and control the shapes of nanoparticles.

Wulff shape can be constructed according to the surface energies, which usually can be obtained by accurate density functional theory (DFT) calculations. For such calculations, there are usually two methods to build the slab. In the first one, the slab is built in the stoichiometry way, and the surface energy is defined as [6]:

$$\gamma = \frac{E_s - NE_b}{2S} \quad (1)$$

where γ, E_s, E_b, N, and S are the surface energy, the total energy of the slab, the energy of unit cell, the number of unit cell in the constructed slab, and the area of the surface, respectively. Its advantage is that the E_b and E_s can be calculated directly, and it doesn't need any other approximations compared with the non-stoichiometry way. However, in some cases, the up surface is not the same as the bottom surface in the slab, and a dipole electric field would be generated, which doesn't exist in actual nanoparticles [7]. This electric field will bring the extra energy to the E_s term in slab calculation, leading to a bigger surface energy than the real value. Thus the calculated shape would deviate from the actual nanoparticle shape. One way to deal with this problem is to increase the thickness of the slab enough to decrease the dipole electric field, but the corresponding cost for computation would be increased significantly [7]. Moreover, the dipole electric field and the surface energy deviation still exist.

For the second method, the slab is built in a non-stoichiometry way. If the dipole electric field exists in the stoichiometry slab, one layer or few layers of atoms can be added to one side of the surface to make the outmost atoms of the two surfaces the same [8]. This could eliminate the dipole electric field, and the surface energy is defined as:

$$\gamma = \frac{E_s - NE_b + \sum_i n_i \mu_i}{2S} \quad (2)$$

where n_i, μ_i, and i are the number of added atoms, the atomic chemical potential, and the species of atoms. In this method, we should estimate the atomic chemical potentials that the added atoms bring about. Generally, this estimation is not so accurate that it would also bring deviation to the real value of surface energy.

In this work, we develop an improved method through multivariate linear regression to fit the calculated surface energies with no dipole electric field to get the separate contributions to the surface energy from the cations coordination loss terms at the surface. The fitted results can further be used to estimate the surface

---

* Corresponding authors.
E-mail addresses: zhengjx@pku.edu.cn (J. Zheng), panfeng@pku.edu.cn (F. Pan).

http://dx.doi.org/10.1016/j.commatsci.2017.05.025

energies of slabs with dipole electric field accurately. Using this developed method, we study the equilibrium crystal shapes of three different phases of Li_2CoSiO_4 (LCS) named β_{II}-LCS, β_I-LCS, and γ_0-LCS (Fig. S1 in Supplementary Materials), respectively, which belong to a large family of materials known as the tetrahedral structures and are a kind of recently widely studied cobalt redox-active electrode materials for rechargeable lithium batteries [9–11]. They also show a great potential for oxygen evolution reaction (OER) electrocatalysts, thus it is worthy studying their equilibrium crystal shapes to know the mainly exposed surfaces where the OER happens.

2. Methods

All calculations in this work are performed using the plane-wave projector-augmented wave method with an energy cut-off of 520 eV, as implemented in the Vienna ab initio simulation package (VASP) [12–16]. The Perdew-Burke-Ernzerhof (PBE) [17] form of GGA was chosen as the exchange-correlation potential. The PBE+U approach was employed to take account of the short on-site Coulomb interaction (U) presented in the localized 3d electrons of Co, with the U values set to 3.32 eV for Co [18]. The structures were relaxed until the forces were less than 0.03 eV/Å, and the energy convergent standard was 10^{-5} eV. The k-point meshes of β_{II}-LCS, β_I-LCS, γ_0-LCS unit cells were set to $5 \times 5 \times 6$, $5 \times 3 \times 6$, $5 \times 3 \times 6$, respectively, and β_{II}-LCS, β_I-LCS, γ_0-LCS belongs to $Pmn2_1$, $Pbn2_1$, $P2_1/n$ space group, respectively. For the β_{II}-LCS phase, we use the anti-site structure reported by experiments. The errors for the calculated lattice constants compared with the XRD data for three phases are lower than 1.6% (Supplementary Materials Table S1–S3). A vacuum buffer space of at least 15 Å is set for all slabs.

We investigated all the basic low index faces ((100), (010), (001), (110), (101), (011), and (111)) and some other possible high index faces with low surface energies (e.g., (120), (210), and (130)). The general rule of cutting face should minimize the ion coordination loss at the surface. We performed crystal orbital Hamilton populations (COHP) [19,20] bond analysis in the unit cell of β_{II}-LCS (Table S4), which can be used to estimate the bond strength. The results show that the strength of Si—O, Co—O, and Li—O bonds follows: Si—O > Co—O > Li—O, and the bond length also follows this trend. For the situation of LCS materials, the rules are:

(1) For the same cutting plane with different terminal atoms, we choose the way that breaks less bonds as far as possible;
(2) The breaking of Si—O bond would increase the surface energy greatly, so we choose the way that does not break the Si—O bond as far as possible;
(3) If the number of the broken Co—O bonds is the same with the broken Li—O bonds, we choose to break Li—O bonds, as the Li—O bonds are weaker than the Co—O bonds;
(4) In some faces, we choose the zigzag way to minimize the number of broken bonds;
(5) The priority of the above four rules decreases successively.

Because the surfaces with dipole electric field would reconstruct beyond simple geometrical relaxations, we also have calculated the surface energies using a larger slab (2×2 of primary slab) for β_{II}-LCS phase (Table S5), and found that the difference between the results from primary slab and the results from the larger slab is quite small.

3. Results and discussion

All the three structures (β_{II}-LCS, β_I-LCS, γ_0-LCS) we studied are vertex-connected tetrahedron networks. Different from the full octahedron (e.g., layered $LiMO_2$) and octahedron/tetrahedron hybrid structures (e.g., Co_3O_4 and olivine $LiCoPO_4$) with coplanar or collinear, the cobalt tetrahedra are cross-linked by silicate groups in LCS. Fig. 1 shows the atomic structure and the examples of cutting planes of β_{II}-LCS. We take the stoichiometry ratio way to cut the lattice plane, which guarantees the electric neutrality of slab. Almost half of the slabs with no perpendicular dipole belong to the "type I" and the "type II" surfaces [21], and dipole exists on another half of slabs along the direction of the surface normal, including some vanishing dipole slabs and great dipole slabs. We considered all the different situations in three different phases. There are two non-equivalent ways to cut the (010) lattice plane (Fig. 1b), which would lead to different terminated atoms. Specifically, the (010)-1 cutting way breaks the Si—O bonds and the Li—O bonds, and the (010)-2 cutting way breaks the Co—O bonds and the Li—O bonds. Our calculations show that the surface energy of (010)-2 is smaller than (010)-1, so we use the data of (010)-2 as the final data for Wulff construction. For (100) and (001) lattice plane, there is only one non-equivalence cutting way.

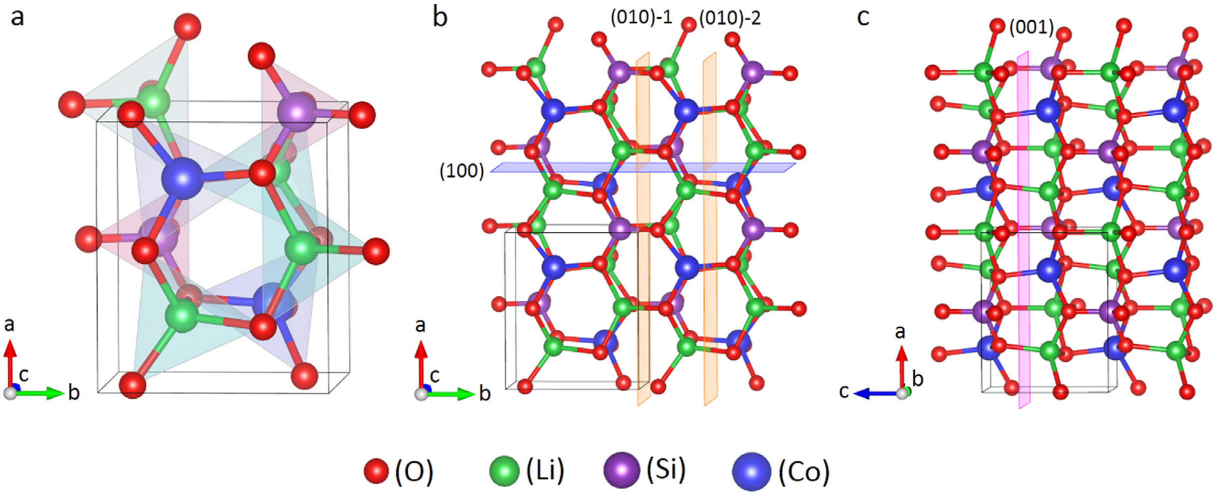

Fig. 1. (a) The unit cell of β_{II}-LCS phase. (b) The cutting way of (010) and (100) lattice plane of β_{II}-LCS phase. (010)-1 and (010)-2 are two non-equivalence ways of cutting (010) lattice plane. (c) The cutting way of (001) lattice plane of β_{II}-LCS phase.

Fig. 2 is a slab model for surface energy calculation. The surface terminated cations would present net positive charge compared with the cations in the bulk after electronic structure optimization, and we use "+" to denote this net charge. Due to the same terminated atomic species and corresponding atom number between the up surface and bottom surface (Fig. 2a), (010)-2 slab is a non-dipole slab, so the surface energy of this kind of slabs can be calculated directly and accurately. For the (100) slab (Fig. 2b), the terminal atoms are Co, Li, and O for the upper surface and Si, Li, and O for the bottom surface. Due to the different valence states of Co (2+) and Si (4+), a weak dipole electric field will be generated, and the total energy of the surface slab (E_s) would deviate a little from the situation with no dipole electric field. In Fig. 2c, for the (001) slab, one surface of slab is terminated with anions (O), and the other one is terminated with cations (Co, Si, Li), thus great net charge exists on both surfaces after relax and electric structure optimization and a great dipole electric field is generated. In this condition, a great error will be brought to E_s term for surface energy calculation. Table 1–3 show the details of the dipole electric field in selected surfaces for three phases. We rule out all the (101), (001), and (111) slabs of three phases, because the density of broken bond is apparently higher than other faces, leading to high surface energies (Table 4).

As breaking a chemical bond would lead to cation coordination loss and extra surface energy during cutting the plane, we try to quantify the surface energy contributions from every kind of cation coordination loss. For the vertex-connected tetrahedron networks of all three Li_2CoSiO_4 phases we considered, it just needs to break one bond for every cation coordination (CoO_4, SiO_4, and LiO_4) to cut low-index lattice planes and some high-index lattice planes, forming cations coordination loss (CoO_3, SiO_3, and LiO_3) on the slab surface (Fig. 2). So we have three variables. At the same time, there exist some slabs with no dipole electric field, and the surface energy can be accurately calculated. When the number of this kind

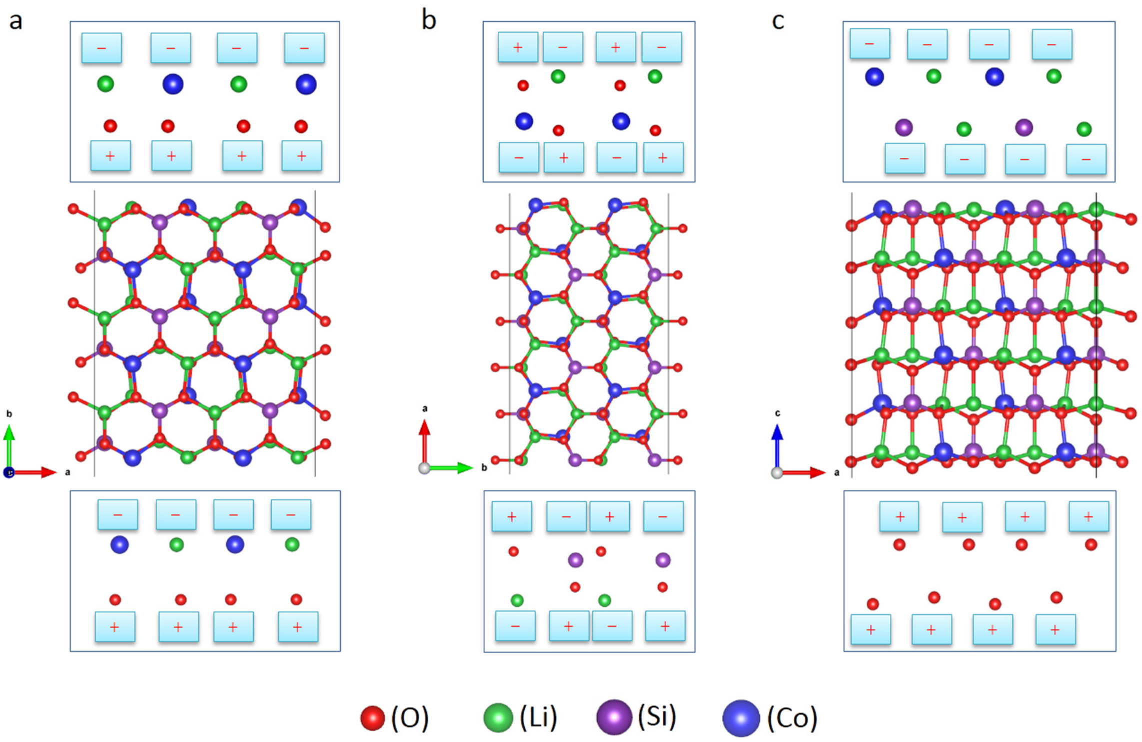

Fig. 2. Slab model and the dipole electric field analysis of three orientations, "+" and "−" are used to denote the charge distribution of relaxed surface atoms relative to the corresponding atoms of bulk. (a) The (010)-2 slab, (b) the (100) slab, (c) the (001) slab.

Table 1
DFT calculated and multivariate linear regression fitted results of β_{II}-LCS phase. n_O is the number of exposed OM_3 (M = Si, Co and Li), and DEF is the acronym of dipole electric field.

Lattice plane	Surface	n_{Si}	n_{Co}	n_{Li}	n_O	DEF	E_s-NE_b (eV)	Fitting	Fitting (total)	Relative error (%)
(010)-1	Up	1	/	1	2	No	8.30	4.15	8.30	0.0
	Down	1	/	1	2			4.15		
(010)-2	Up	/	1	1	2	No	3.10	1.41	2.82	9.0
	Down	/	1	1	2			1.41		
(210)	Up	1	1	2	4	No	10.95	5.56	11.12	1.6
	Down	1	1	2	4			5.56		
(100)	Up	1	/	1	2	Weak	5.53	4.15	5.56	0.5
	Down	/	1	1	2			1.41		
(110)	Up	/	2	1	3	Weak	4.49	2.28	3.89	13.4
	Down	/	/	3	3			1.61		
(001)	Up	1	1	2	/	Strong	7.65	5.56	5.56	27.3
	Down	/	/	/	4			0		

Table 2
DFT calculated and multivariate linear regression fitted results of β_I-LCS phase. n_O is the number of exposed OM_3 (M = Si, Co and Li), and DEF is the acronym of dipole electric field.

Lattice plane	Surface	n_{Si}	n_{Co}	n_{Li}	n_O	DEF	E_s-NE_b (eV)	Fitting	Fitting (total)	Relative error (%)
(010)-1	Up	1	/	1	2	No	8.30	4.15	8.30	0.0
	Down	1	/	1	2			4.15		
(010)-2	Up	/	1	1	2	No	3.15	1.41	2.82	10.5
	Down	/	1	1	2			1.41		
(110)-1	Up	1	/	3	4	No	10.39	5.23	10.46	0.7
	Down	1	/	3	4			5.23		
(110)-2	Up	1	2	1	4	No	11.48	5.90	11.8	2.8
	Down	1	2	1	4			5.90		
(120)	Up	/	2	4	6	No	7.52	3.89	7.78	3.5
	Down	/	2	4	6			3.89		
(100)	Up	2	/	2	4	Weak	10.55	8.30	11.12	5.4
	Down	/	2	2	4			2.82		
(210)	Up	1	3	4	8	Weak	20.35	8.38	22.25	9.3
	Down	3	1	4	8			13.87		
(001)	Up	2	2	4	/	Strong	15.30	11.12	11.12	27.3
	Down	/	/	/	8			0		

Table 3
DFT calculated and multivariate linear regression fitted results of γ_0-LCS phase. n_O is the number of exposed OM_3 (M = Si, Co and Li), and DEF is the acronym of dipole electric field.

Lattice plane	Surface	n_{Si}	n_{Co}	n_{Li}	n_O	DEF	E_s-NE_b (eV)	Fitting	Fitting (total)	Relative error (%)
(001)	Up	1	1	2	4	No	11.60	5.56	11.12	4.1
	Down	1	1	2	4			5.56		
(010)-1	Up	1	/	1	2	No	8.63	4.15	8.30	3.8
	Down	1	/	1	2			4.15		
(010)-2	Up	/	1	1	2	No	3.13	1.41	2.82	9.9
	Down	/	1	1	2			1.41		
(110)-1	Up	1	/	3	4	No	10.30	5.23	10.46	1.6
	Down	1	/	3	4			5.23		
(110)-2	Up	1	2	1	4	No	11.70	5.90	11.80	0.8
	Down	1	2	1	4			5.90		
(120)	Up	/	2	4	6	No	7.85	3.89	7.78	0.9
	Down	/	2	4	6			3.89		
(100)	Up	2	/	2	4	Weak	10.60	8.30	11.12	4.9
	Down	/	2	2	4			2.82		
(210)	Up	1	3	4	8	Weak	20.39	8.38	22.25	9.1
	Down	3	1	4	8			13.87		
(130)	Up	2	0	6	8	Weak	22.52	11.80	19.58	13
	Down	2	4	2	8			7.78		

of slabs is equal to or exceeds the number the variables, the surface energies of slabs with no dipoles can be fitted to find out whether the three variables are independent. Use the multivariate linear regression method, we further fit these three variables:

$$E_s - NE_b = n_{C0}x_{C0} + n_{Si}x_{Si} + n_{Li}x_{Li} \tag{3}$$

n_{Co}, n_{Si}, and n_{Li} are the number of CoO_3, SiO_3, and LiO_3 on the surface of slab, respectively (Table 1–3), and x_{Co}, x_{Si}, and x_{Li} are the fitting variables corresponding to the surface energy contributions from CoO_3, SiO_3, and LiO_3, respectively. For easy viewing, we extend the slab twofold in the horizontal direction. As an example, in the actual slab of (010)-2 orientation (Fig. 2a), n_{Co}, n_{Si}, and n_{Li} are 1, 0, and 1, respectively.

After fitting the total energies of all lattice slabs with no dipole electric field for three phases, we get $x_{Co} = 0.87$, $x_{Si} = 3.62$, and $x_{Li} = 0.54$, respectively. The fitting errors for the above three terms are 4.4%, 5.9%, and 2.9%, respectively, and the R-square was 0.999, indicating a well linear dependence. These results also show that the contributions to the surface energy from the exposed CoO_3, SiO_3, and LiO_3 of different phases or structures is relative stable. Based on these results, we can build a data base using the fitted data from slabs with no dipole field and use them to estimate the surface energy for every possible surface directly. The fitted results indicate that the SiO_3 is the main source of the surface energy. It should be mentioned that as broking Si—O bond would bring great surface energy, we initially tried to keep the complete SiO_4 tetrahedral structure without breaking Si—O bonds when we cut the surface. Nevertheless, it was found that this way would bring even larger surface energy than the way of cutting one Si—O bond from SiO_4 to form SiO_3 structure on the exposed surface. So we adopt the data of SiO_3 in our later fitting to estimate the surface energies of slabs with weak dipole and great dipole. Form Tables 1–3, we can see that except for the (010)-2 surface, for the surfaces without dipole field, the surface energies estimated from the fitted data are close to the directly calculated values. The fitting surface energy of all (010)-2 face in three phases deviated from the directly calculated value by about 10%, which originates from the relative larger surface reconstruction after relaxation. While for the surfaces with weak or strong dipole field, the estimated values from fitted data show a great deviation compared with the directly

Table 4
Calculated surface energies for three phases using the multivariate linear regression method.

γ (J/m^2)	(010)-2	(001)	(100)	(210)	(110)	(101)	(011)	(111)	(120)	(130)
β_{II}-LCS	0.78	1.31	0.84	1.4	0.86	1.01	1.51	1.51	1.47	/
β_{I}-LCS	0.80	1.31	0.84	1.19	1.33	1.03	1.60	1.50	0.72	/
γ_0-LCS	0.78	1.30	0.82	1.17	1.29	1.13	1.13	1.57	0.74	1.50

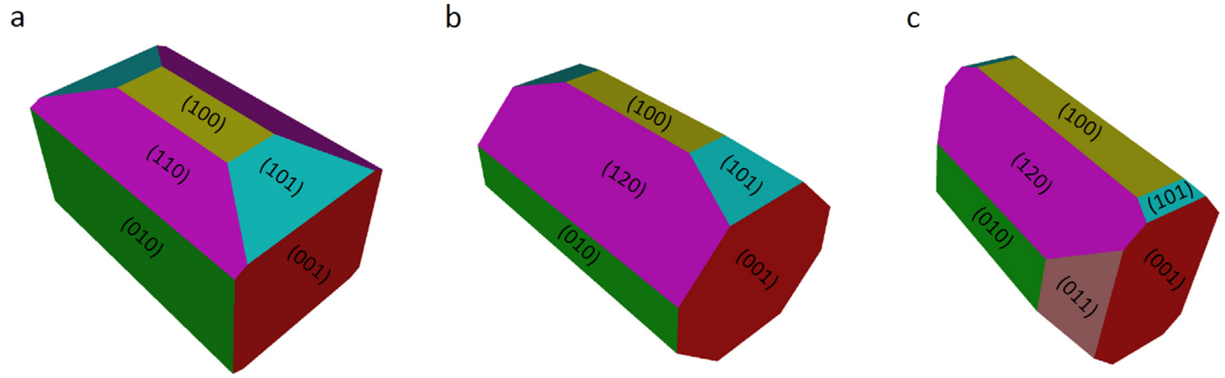

Fig. 3. (a) Wulff shape of β_{II}-LCS phase using the calculated surface energy, (b) Wulff shape of β_{I}-LCS phase, (c) Wulff shape of γ_0-LCS phase.

calculated values. Specifically, the deviation between the directly calculated data and the fitted data for the weakly polarized surface is under 14%, and the deviation for the completely polarized surface is almost 30%. These results suggest that the directly calculated data of the surface with dipole field can't be used for Wulff shape prediction. Table S5–7 shows a comparison between the surface energies without and with adopting the dipole correction schemes implemented in VASP [7,22]. It can be seen that there is little difference between the calculated surface energies with and without dipole correction, indicating that our method outperforms the dipole correction method in VASP to correct the dipole field for LCS slabs.

Table 4 shows the final calculated surface energies of three phases, and the surface energies with weak and strong dipole electric field are estimated using the fitted surface energy contributions from CoO_3, SiO_3, and LiO_3. Finally, using the above calculated surface energies, we draw the Wulff shape for the three phases of LCS using the Wulffman visual software (Fig. 3). We can see that (100), (010), (001), (110), (110) are the exposed surfaces in β_{II}-LCS phase, and (100), (010), (001), (120), (110) are the exposed surfaces in β_{I}-LCS phase, and (100), (010), (001), (120), (101), (011) are the exposed surfaces in γ_0-LCS phase. The largest exposed surfaces of β_{II}-LCS phase, β_{I}-LCS phase, γ_0-LCS phase are (010), (120), and (120), respectively, and they just break the Co—O, Li—O bonds, and no Si—O bond is broken. This confirms that the Si—O bond is stronger than Co—O bond and Li—O bond, and breaking stronger bond would bring larger surface energy. Interestingly, the (001) surfaces of all three phases have relative big exposed surface even though they have relative large surface energies. This can be explained that compared with other planes with the same plane index (e.g., (101), (011), and (111)) in three phases, the surface energies of (001) surfaces are lower than those of (011) and (111) surfaces. Though the surface energies of (101) surfaces are lower than those of (001) surfaces, the (101) surfaces have to compete with (100), (110), and (120) surfaces, which all have relative lower surface energies. Especially, (011) surface appears in the Wulff shape of γ_0-LCS phase, because it has relative lower surface energy compared with other two phases. (101) surfaces exist on the Wulff shape for all three phases, because of their relative low surface energies.

4. Conclusion

We used the multivariate linear regression to fit the calculated surface energies of slabs with no dipole electric field for β_{II}-LCS, β_{I}-LCS, and γ_0-LCS, and found that the surface energy contributions from CoO_3, SiO_3, and LiO_3 show a great linear dependence. The fitted results from surfaces without dipoles can be used to estimate the surface energies of slabs with weak and strong dipole field directly and accurately. Our proposed multivariate regression could be applied to other tetrahedral structure systems, but for systems with other types of arrangements (e.g., octahedral, trigonal, or even mixtures of them), its application depends on whether the number of slabs with no dipole electric field is equal or exceeds the number of variables for cations coordination loss and needs further tests.

Acknowledgement

The work was financially supported by National Materials Genome Project (2016YFB0700600), the National Natural Science Foundation of China (No. 21603007), and Guangdong Innovation Team Project (No. 2013N080), Shenzhen Science and Technology Research Grant (No. ZDSY20130331145131323, JCYJ20140903101633318, JCYJ2014090-3101617271).

Appendix A. Supplementary material

Supplementary data associated with this article can be found, in the online version, at http://dx.doi.org/10.1016/j.commatsci.2017.05.025.

References

[1] E. Ringe, R.P. Van Duyne, L.D. Marks, Kinetic and thermodynamic modified Wulff constructions for twinned nanoparticles, J. Phys. Chem. C 117 (31) (2013) 15859–15870.
[2] L. Mayrhofer et al., Fluorine-terminated diamond surfaces as dense dipole lattices: the electrostatic origin of polar hydrophobicity, J. Am. Chem. Soc. 138 (12) (2016) 4018–4028.
[3] E. Ringe, R.P. Van Duyne, L.D. Marks, Wulff construction for alloy nanoparticles, Nano Lett. 11 (8) (2011) 3399–3403.

[4] J.G. Che et al., Surface atomic structures, surface energies, and equilibrium crystal shape of molybdenum, Phys. Rev. B 57 (3) (1998) 1875–1880.

[5] H.G. Yang et al., Anatase TiO_2 single crystals with a large percentage of reactive facets, Nature 453 (7195) (2008) 638–641.

[6] D. Zherebetskyy et al., Hydroxylation of the surface of PbS nanocrystals passivated with oleic acid, Science 344 (6190) (2014) 1380–1384.

[7] G. Makov, M.C. Payne, Periodic boundary conditions in ab initio calculations, Phys. Rev. B 51 (7) (1995) 4014–4022.

[8] H. Kim et al., Coordination tuning of cobalt phosphates towards efficient water oxidation catalyst, Nat. Commun. 6 (2015) 8253.

[9] A.R. Armstrong et al., Structural polymorphism in Li_2CoSiO_4 intercalation electrodes: a combined diffraction and NMR study, Chem. Mater. 22 (5) (2010) 1892–1900.

[10] G. He, G. Popov, L.F. Nazar, Hydrothermal synthesis and electrochemical properties of Li_2CoSiO_4/C nanospheres, Chem. Mater. 25 (7) (2013) 1024–1031.

[11] C. Lyness et al., The lithium intercalation compound Li_2CoSiO_4 and its behaviour as a positive electrode for lithium batteries, Chem. Commun. 46 (2007) 4890–4892.

[12] G. Kresse, J. Furthmuller, Efficient iterative schemes for ab initio total-energy calculations using a plane-wave basis set, Phys. Rev. B 54 (16) (1996) 11169–11186.

[13] G. Kresse, J. Furthmuller, Efficiency of ab-initio total energy calculations for metals and semiconductors using a plane-wave basis set, Comput. Mater. Sci. 6 (1) (1996) 15–50.

[14] G. Kresse, J. Hafner, Ab initiomolecular dynamics for liquid metals, Phys. Rev. B 47 (1) (1993) 558–561.

[15] G. Kresse, J. Hafner, Ab initiomolecular-dynamics simulation of the liquid-metal–amorphous-semiconductor transition in germanium, Phys. Rev. B 49 (20) (1994) 14251–14269.

[16] P.E. Blochl, Projector augmented-wave method, Phys. Rev. B: Condens. Matter 50 (24) (1994) 17953–17979.

[17] J.P. Perdew, K. Burke, M. Ernzerhof, Generalized gradient approximation made simple, Phys. Rev. Lett. 77 (18) (1996) 3865–3868.

[18] B. Zhang et al., Homogeneously dispersed multimetal oxygen-evolving catalysts, Science 352 (6283) (2016) 333–337.

[19] V.L. Deringer, A.L. Tchougreeff, R. Dronskowski, Crystal orbital hamilton population (COHP) analysis as projected from plane-wave basis sets, J. Phys. Chem. A 115 (21) (2011) 5461–5466.

[20] S. Maintz et al., LOBSTER: a tool to extract chemical bonding from plane-wave based DFT, J. Comput. Chem. 37 (11) (2016) 1030–1035.

[21] L. Wang et al., First-principles study of surface properties ofLiFePO4: surface energy, structure, Wulff shape, and surface redox potential, Phys. Rev. B 76(16) (2007).

[22] J. Neugebauer, M. Scheffler, Adsorbate-substrate and adsorbate-adsorbate interactions of Na and K adlayers on Al(111), Phys. Rev. B 46 (24) (1992) 16067–16080.